ADVANCED MATERIALS
www.advmat.de

Confined Flash Printing and Synthesis of Stable Perovskite Nanofilms under Ambient Conditions

Yuxin Liu, Tanja Knaus, Zheng Wei, Junfang Zhang, Matteo Damian, Sebastian Ronneberger, Xingjun Zhu, Peter H. Seeberger, Hong Zhang, Francesco G. Mutti,* and Felix F. Loeffler**

The fabrication of stable perovskite nanofilm patterns is important for the development of functional optical devices. However, current production approaches are limited by the requirement for strict inert gas protection and long processing times. Here, a confined flash printing synthesis method is presented to generate perovskite nanofilms under ambient conditions, combining precursor transfer, perovskite synthesis, crystallization, and polymer protection in a single step within milliseconds. A laser simultaneously prints and induces the flash synthesis, confined in a polymer nanofilm, under normal ambient conditions. Due to its simplicity and flexibility, the method enables the combination and screening of many different perovskite precursor materials on various substrates. Besides for the development of novel perovskite materials and devices, the nanofilms can be applied for biodetection. The unique H_2O_2-responsive property of the ultrathin perovskite quantum dot film is applied for biomolecule detection based on oxidase-catalyzed enzymatic reactions.

1. Introduction

Perovskite quantum dot (PQD) films have been extensively explored for the fabrication of advanced optical devices such as solar cells,[1] lasers,[2] sensors,[3] and light-emitting diodes (LEDs).[4] However, due to their low formation energy, PQDs are fragile and therefore unstable when exposed to oxygen or moisture.[5] To meet the demands of various applications, stable polymer-coated PQD films must be fabricated under inert gas protection.[6–8] The most commonly used approach today typically involves multiple processing steps in an inert gas-filled glove box, requiring strict fabrication conditions, high-end settings, and complex procedures that have long been considered as the key obstacles for upscaling.[9–11] While a recently reported approach can enable perovskite formation under normal lab conditions, it still requires precursor mixing and preparation steps under strict inert conditions.[12] Only one approach circumvents this issue by doping the precursors into glass, but this restricts it to inorganic perovskites with very limited application as the perovskite is embedded in glass.[13,14] Thus, all recently reported material-flexible methods require pre-mixing of precursors under inert gas protection using anhydrous solvents (**Table 1**).[15–18] In addition, it is challenging to fabricate arbitrary PQD films patterns without suffering from slow fabrication in the range of hours, due to low printing speed (e.g., lithography) or prolonged annealing times

Y. Liu, J. Zhang, S. Ronneberger, P. H. Seeberger, F. F. Loeffler
Department of Biomolecular System
Max Planck Institute for Colloids and Interfaces
14476 Potsdam, Germany
E-mail: Felix.Loeffler@mpikg.mpg.de

Y. Liu, T. Knaus, Z. Wei, M. Damian, H. Zhang, F. G. Mutti
Van 't Hoff Institute for Molecular Sciences
University of Amsterdam
Science Park 904, Amsterdam 1098 XH, The Netherlands
E-mail: H.Zhang@uva.nl; F.Mutti@uva.nl

The ORCID identification number(s) for the author(s) of this article can be found under https://doi.org/10.1002/adma.202409592

DOI: 10.1002/adma.202409592

Y. Liu, P. H. Seeberger
Institute of Chemistry and Biochemistry
Free University of Berlin
14195 Berlin, Germany

S. Ronneberger
Institute of Physics and Astronomy
University of Potsdam
Campus Golm
14476 Potsdam, Germany

X. Zhu
School of Physical Science and Technology
State Key Laboratory of Advanced Medical Materials and Devices
ShanghaiTech University
Shanghai 201210, China

Table 1. Recently reported methods for fabricating PQD films.

Method	No inert gas and/or anhydrous solvents	Patternable	Material and application scope
Spin-coating[12]	✗	✗	✓
CVD[17]	✗	✗	✓
Press printing[16]	✗	✗	✓
Doctor blade[19]	✗	✓	✓
Laser heating[14]	✓	✓	✗
Squeeze blade[15]	✗	✗	✓
In situ coating[21]	✗	✗	✓
Polymer pen lithography[22]	✗	✓	✓
This work	✓	✓	✓

(e.g., doctor blade) (Table 1, column 3).[19–21] Moreover, most current methods do not allow for a nanoscale control of a protective polymer coating, preventing these PQD films from being used in applications that require mass transfer (e.g., biodetection). While a typical micrometer thick protective polymer coating is beneficial for the PQD stability, it also blocks potentially desired interactions with the PQDs.

To address these critical issues, we demonstrate the confined flash printing (conFlash) synthesis of PQDs within a polymer nanofilm. Based on laser-induced forward transfer (LIFT) of thin films with integrated flash heating, our conFlash approach enables the synthesis of organic–inorganic hybrid as well as purely inorganic PQD nanofilm patterns within milliseconds. This is an additive manufacturing approach that uses focused laser irradiation to achieve the transfer and in situ mixing of different polymer layers containing the individual precursors. The spatial separation of metal ions and halide precursors is the critical step that allows us to perform the process under normal lab conditions using standard solvents without the inherent risk of decomposition when using pre-mixed precursors. Therefore, the much easier fabrication requirements, the high printing/synthesis speed, and the wide range of precursors and materials are major advantages of our conFlash synthesis. Furthermore, our conFlash approach provides a practical solution to the challenges of pattern generation and controlled polymer protection. By programming the laser scan pattern, speed, and laser power, we can control the position and amount of transferred precursor-containing polymer, as well as the confined precursor mixing to synthesize PQDs. As a result, we can realize the rapid synthesis of arbitrary PQD nanofilm patterns and tune their thickness at the nanoscale to enable selective molecular interaction for biodetection.

2. Results

The conFlash synthesis of PQDs by LIFT involves two main steps: i) stable immobilization of metal ions on a substrate and ii) synthesis of PQDs in a hydrophobic polymer nanofilm. For the first step, we immobilize metal ions (e.g., Pb^{2+}) on the substrate by an alginate-metal hydrogel.[23] Therefore, alginate is spin-coated on a substrate, and then, the Pb^{2+} in polyethylene glycol (PEG) is laser-transferred to the alginate-coated substrate (**Figure 1**A). Under the optimal temperature and in presence of water vapor, the carboxyl groups from the alginate coordinate with Pb^{2+}, rapidly forming a stable hydrogel on the substrate (Figure S1, Supporting Information).[24–26] The PEG serves as both a vehicle (solid solvent) during laser transfer, as well as a solvent together with the water vapor, forming a nanoreactor for Pb^{2+}-alginate hydrogel formation. After thorough washing to remove unreacted Pb^{2+}, significantly more Pb^{2+} could be observed on the patterned hydrogel than on the non-patterned regions (Figures S2 and S3, Supporting Information). Notably, this metal-hydrogel strategy is universal, allowing the substrate to provide various different metal ions for the preparation of different PQDs (Figure S4, Supporting Information).

With the metal ion-modified substrate, the second step of PQD formation is investigated, where methylammonium lead bromide ($MAPbBr_3$) PQD is chosen as a model (Figure 1B). A hydrophobic polystyrene-poly(butyl acrylate) copolymer (S-LEC) layer containing methylammonium bromide (MABr) is selectively transferred to the Pb^{2+}-bearing substrate, which forms a nanofilm on the substrate and serves as a nanofilm reactor for the confined synthesis of PQDs. During the LIFT process, the laser induces a flash heating, reaching 200 °C within milliseconds (Figure S5, Supporting Information), which melts and transfers the MABr-containing polymer layer and generates a nanofilm on the Pb^{2+}-modified substrate.[27] This allows us to prepare PQD nanofilms in milliseconds, significantly reducing fabrication time (vs hours or days using traditional methods with post-processing).[28,29] In addition, since the mixing and reaction of precursors takes place in the polymer film, there is no need for inert gas protection or the use of anhydrous solvents as in conventional spin-coating or blading methods.[12,15,19] By using different laser parameters (e.g., laser power density and scanning speed), the microstructure (Figure S6, Supporting Information), thickness (2.5–131.5 nm, Figure S7, Supporting Information), flatness (0.5–177.6 nm, Figure S8, Supporting Information), and fluorescence intensity (Figure S9, Supporting Information) of the nanofilm can be modulated to suit various applications. It is worth noting that above a certain laser energy threshold, the generated fluorescence intensity of the PQD films decreases with increasing laser energy/heat because of partial decomposition of MABr. By tuning the laser parameters, we can obtain PQD nanofilms with or without microstructures and at the same time realize the patterning of PQD nanofilms for different application scenarios (Figure 1C,D). Notably, multiple nanofilms of similar thickness can be generated rapidly and reproducibly, but each with a physically random microstructure, which allows for their unique identification (Figure S10 and S11, Supporting

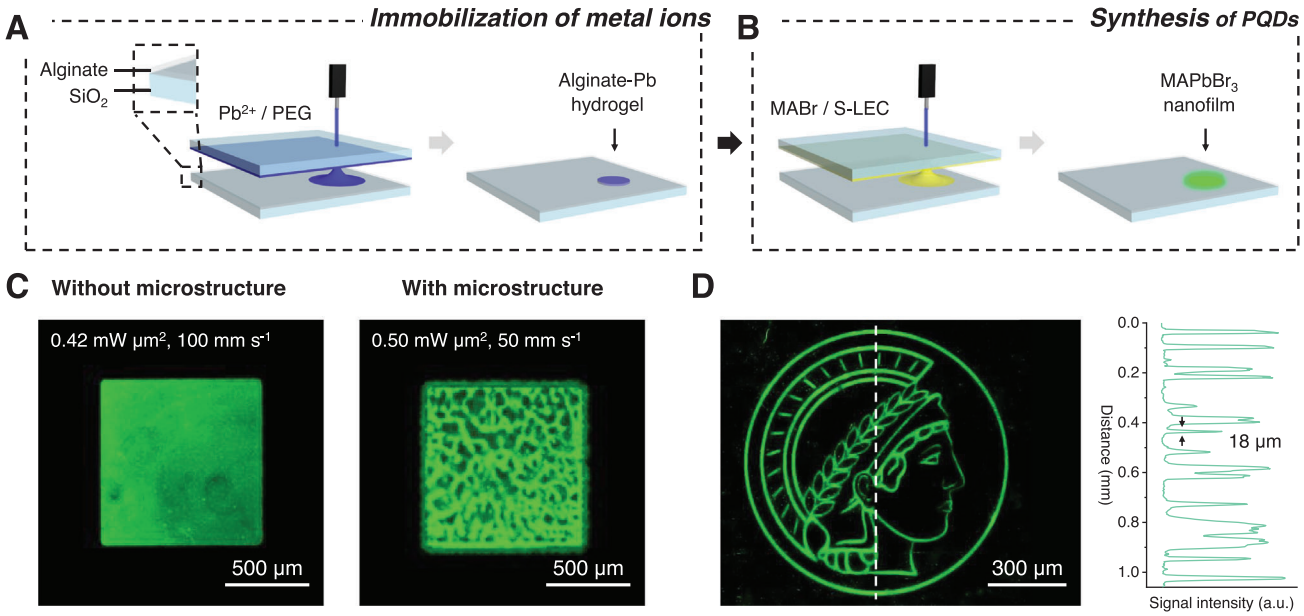

Figure 1. Confined flash printing (conFlash) synthesis of PQDs in a polymer nanofilm. A,B) Scheme, showing the stepwise conFlash synthesis of PQD: A) selective immobilization of metal ions on a substrate and B) synthesis of PQDs in a hydrophobic polymer nanofilm. C) Fluorescence images of patterns without (left) and with microstructure (right) controllably prepared by different laser parameters, represented using the same linear fluorescence intensity scale. Average film thicknesses without microstructure ≈4 nm, with microstructure ≈17 nm. D) Fluorescence image (left) and signal distribution (right) of a patterned PQD nanofilm. Signal distribution paths are indicated in the fluorescence image by a dotted white line. Minimum line feature down to ≈18 µm.

Information).[30] Based on the fluorescence intensity and the characteristic microstructure, we selected those laser parameters that generate macroscopically homogeneous and flat nanofilms with microstructures, which will increase the relative surface area and benefit certain applications (**Figure** 2A,B).

Upon flash heating, the PQDs are synthesized and dispersed in the hydrophobic polymer nanofilm. Benefiting from the confined synthesis in the nanofilm, the synthesized PQDs are ultrasmall (<10 nm) (Figure 2C). The Pb(4f) and N(1s) X-ray photoelectron spectra of the nanofilm show typical signature peaks of $MAPbBr_3$ QDs, as reported by others (Figure 2D; Figure S12, Supporting Information).[31] Although transparent in the visible range, the nanofilms absorb at wavelengths <520 nm (Figure 2E) and show a bandgap of 2.23 eV (Figure S13A, Supporting Information), which is similar to a spin-coated $MAPbBr_3$ PQD film, prepared by the conventional method of pre-synthesized PQDs in a glove box (Figures S13B and S14, Supporting Information). The PQD nanofilm fluoresces, showing a lifetime of 8.3 ns with an emission peak at 533.6 nm, and a full width at half maximum of 27.9 nm (Figures S13C and S15, Supporting Information). Therefore, the $MAPbBr_3$ PQDs generated by the conFlash synthesis method show comparable optical properties to the conventionally prepared PQD material (Figure S13B,D, Supporting Information). In addition, the photoluminescence quantum yield for the $MAPbBr_3$ nanofilm is tested to be 36.4 ± 5.1%, which is comparable to the previously reported materials.[32–34]

Furthermore, the conFlash synthesis method is universally applicable to other perovskite types, enabling a PQD synthesis screening approach. The halide anions can be substituted by other methylammonium halide precursors. A series of PQDs from $MAPbCl_xBr_{3-x}$ to $MAPbBr_{3-x}I_x$ (x = 3, 2, 1, and 0) were generated with different Cl/Br and Br/I ratios (**Figure** 3A), resulting in tunable fluorescence peaks between 432–664 nm. Similarly, different cations can be used for the synthesis (Figure 3B), such as methylammonium (MA^+), formamidinium (FA^+), and cesium (Cs^+), indicating that both pure inorganic and hybrid PQDs can be prepared by the conFlash synthesis method. More importantly, the PQDs with multiple cations can also be generated, which further expanded material scope for screening and applications (Figure S16, Supporting Information). In addition, this synthesis method is not only applicable to glass substrates, but also to various functional substrate (e.g., plastic and ITO), which makes it useful for constructing devices for various applications in comparison to traditional laser heating/annealing methods (Figure 3C).[13,14]

Since PQDs hydrate and decompose quickly in a humid environment, they require a polymer protection (Figure S17, Supporting Information). In our case, the PQDs are prepared in situ by the conFlash synthesis method in a hydrophobic polymer with a ten times increased half-life, making the PQD nanofilm stable for >15 days at ambient conditions (**Figure** 4A,B). Notably, compared with typical micro- to millimeter-thick protective hydrophobic polymer coatings, the nanometer-thin layer only slows down instead of completely blocking the penetration of water (Figure 4C). As a result, the PQDs in the nanofilm can interact with solutes from an aqueous solution, which enables us to use the PQD nanofilm as a fluorescence sensor for biodetection and serodiagnostics. This offers a simple approach to fabricate PQD nanofilms without inert gas protection and expand their application field, which is not feasible by previously reported methods.

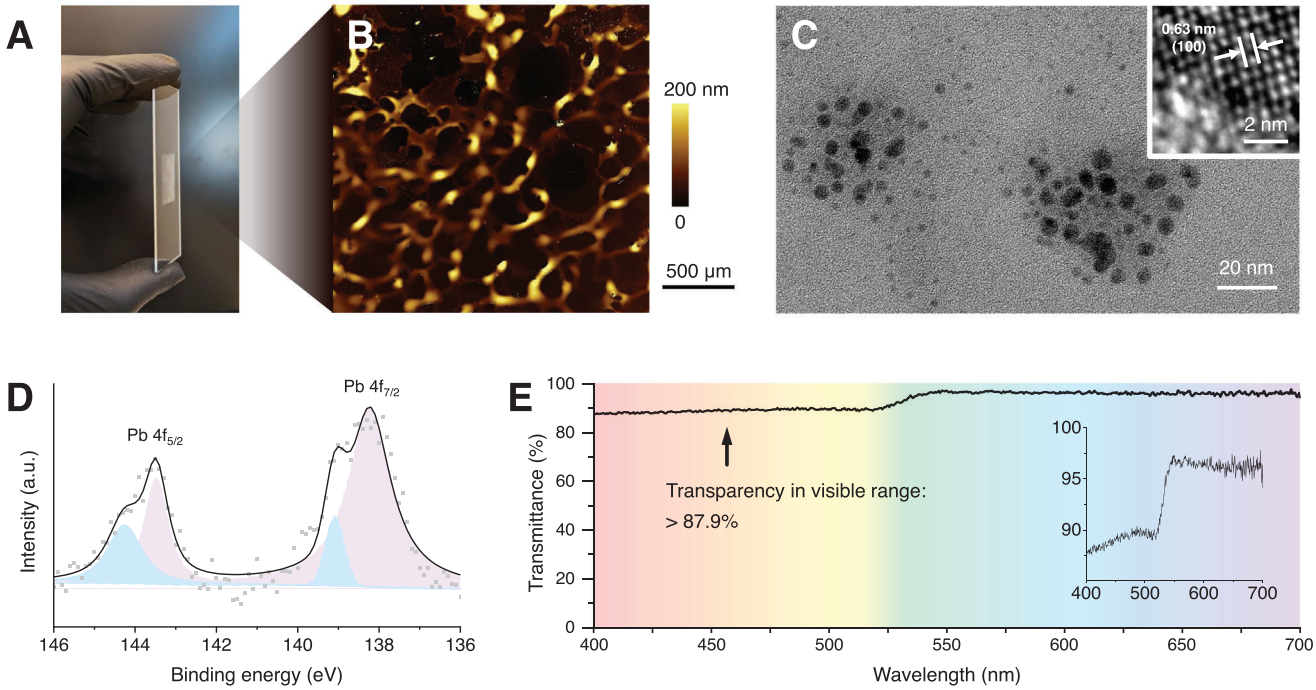

Figure 2. PQDs nanofilm generated by optimal laser parameters. A) Photograph and B) vertical scanning interferometry height measurement of a nanofilm containing $MAPbBr_3$ QDs on a glass slide. C) Transmission electron microscopy image of $MAPbBr_3$ QDs synthesized in a nanofilm, collected from a glass slide by solvent washing, and a high-resolution lattice image insert. D) Pb $4f_{5/2}$ and $4f_{7/2}$ X-ray photoelectron spectrum and E) UV—vis–NIR transmittance spectrum of a nanofilm on a glass substrate.

Compared with water, H_2O_2 decomposes PQDs much more effectively due to a synergistic decomposition effect: hydroxyl radicals and ions are simultaneously produced by the PQD-catalyzed decomposition of H_2O_2, which oxidizes the MA^+ and precipitates the Pb^{2+}, respectively.[35,36] Therefore, the fluorescence of the PQD film is quenched in response to H_2O_2 in aqueous solution (Figure 4D) and is hardly affected by the solvent or other typical biomolecules in serum (Figure S18, Supporting Information). Since lead ions mainly precipitate in the form of hydroxides (Figure S19, Supporting Information), the possibility of lead ion leakage as well as the risk to the environment and operators is minimal. The quenched fluorescence intensity is logarithmically related to the H_2O_2 concentration in the typical biologically relevant range (0–50 μM), which allows the quantification of H_2O_2 (Figure 4E,F).

Owing to their selective H_2O_2-responsive fluorescence, the PQD nanofilms can detect H_2O_2 in biological samples. The films can be printed as an array or arbitrary patterns for simultaneous quantification of multiple samples, while the incubation with a sample does not affect its morphology (Figure S20, Supporting Information). On the one hand, its unique microstructure can serve as a unique (unclonable) label, which helps to identify the samples and reduces mistakes (**Figure** 5A). On the other hand, the PQD nanofilm can also be used to detect other biomolecules by using various enzymes that produce H_2O_2 as a by-product (Figure 5B). As a proof of concept, a 3 × 3 array of PQD nanofilm was printed and incubated with multiple samples. The fluorescence image allows direct and rapid screening of the H_2O_2 concentration (Figure 5C), while the fluorescence profiles provide a quantitative result (Figure 5D). Next, the PQD nanofilms were used for the detection of uric acid, nicotinamide adenine dinucleotide phosphate (NADPH), and phenethylamine, by using engineered uric acid oxidase from *Bacillus* sp. (PDB No. 5AYJ, abbreviated BTUO), NADPH oxidase from *Bacillus subtilis* (PDB No. 1ZCH, abbreviated YcnD), and an engineered monoamine oxidase from *Aspergillus niger* (PDB No. 2VVM, abbreviated MAO-N-D5) as biocatalysts, respectively (Figure 5E; Figure S21, Supporting Information). Due to the generation of H_2O_2 in the enzymatic reactions, the fluorescence of the PQD nanofilms is quenched in response to the studied model disease biomarker, co-enzyme factor, and molecular medicine, indicating a wide applicability of the PQD nanofilm in biodetection and serodiagnostics.

3. Conclusion

In conclusion, we propose the first practical method for fabricating stable PQD nanofilms in situ without inert gas protection or the use of anhydrous organic solvents. PQDs are synthesized in a nanometer confined film within milliseconds by a laser-induced flash heating process and simultaneously protected by a hydrophobic polymer nanofilm. By varying the laser parameters, the thickness and flatness of the PQD nanofilm can be modulated, which will be useful for various applications. In addition, the nanometer thin polymer only slows down the water penetration, instead of completely blocking it, thus allowing the interaction between the PQDs and solutes from an aqueous solution. Therefore, biodetection can be realized with a PQD

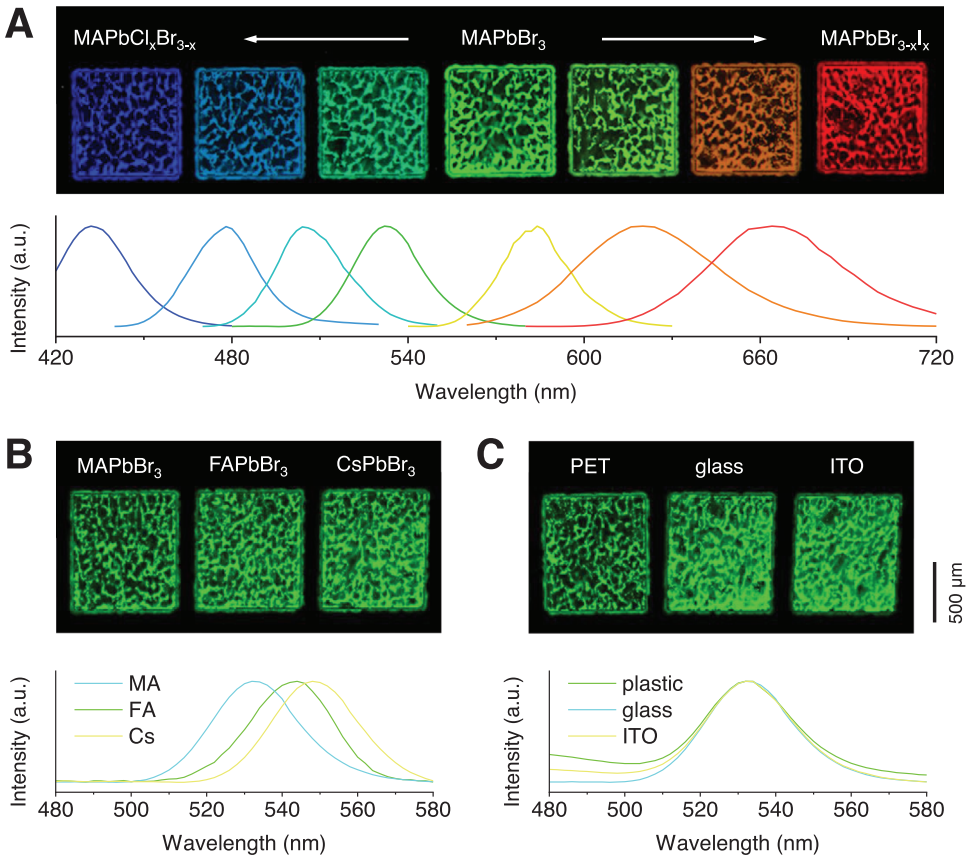

Figure 3. Universality of the conFlash synthesis method. A) Fluorescence image and fluorescence spectra of MAPbCl$_x$Br$_{3-x}$ (x = 3, 2, and 1), MAPbBr$_3$, and MAPbBr$_{3-x}$I$_x$ (x = 1, 2, and 3). The fluorescence image was derived from a single raw image. B) Fluorescence image and fluorescence spectra of MAPbBr$_3$, FAPbBr$_3$, and CsPbBr$_3$ on a glass substrate. C) Fluorescence image and fluorescence spectra of MAPbBr$_3$ on transparent plastic, glass, and ITO substrates.

nanofilm, which is not feasible for films prepared by previously known methods. As a result, our conFlash synthesis method combines the advantages and avoids the drawbacks of the typical PQD synthesis methods. This largely simplifies and reduces PQD production requirements, shortens fabrication times, expands their application field, and gives a universal approach to produce various PQDs on different substrates. Together with robotic automation approaches, the conFlash method will enable reproducible high-throughput synthesis of PQDs by screening a variety of different precursors and substrates.[37] Yet, there are several issues that should be addressed. As shown in Figure 2C, the size distribution of the PQDs is wider than obtained by the well-established solution-based synthesis, due to the weak interaction of our currently used polymers with the precursors, resulting in the widening of fluorescence peaks. In the future, we will try to emulate the liquid-phase synthesis using different polymers or doping ligands into the polymer(s) to obtain more homogeneous PQDs. This will be beneficial to obtain PQD nanofilms with narrower emission peaks. Based on our previous mechanistical studies of our laser-induced forward transfer process,[38–40] we want to further explore advanced variants of light-matter interaction and modify the parameters of this conFlash technique to precisely control the morphology of PQDs. In addition, the amount of PQDs in the nanofilms prepared by the conFlash technique is low. We will address this in our future work by investigating other coating approaches for the donor and acceptor substrate to increase the material layer thicknesses and to study the crystallographic characteristics and optoelectronic properties of the conFlash synthesized PQDs. For biodetection applications, future work should focus on minimizing the impact of the physiological environment on the detection performance of the PQD nanofilms. Therefore, the interaction between the nanofilm and different biomolecules in the physiological environment should be thoroughly investigated, especially potential analytes. Although the analytes studied in this work did not have a significant effect on the fluorescence detection performance of the nanofilms (Figure S22, Supporting Information), it should be advantageous to rationally modify nanofilms (e.g., hydrophilic and hydrophobic modifications by LIFT) and to use more efficient biorecognition groups. In addition, the interaction between biorecognition groups (e.g., enzymes and/or nucleic acids) and PQD nanofilms should be studied in more detail to ensure high sensitivity and selectivity in biodetection.

4. Experimental Section

Materials: The halide precursors MACl, MABr, MAI, and FABr were prepared following previous reports.[32] S-LEC was purchased from

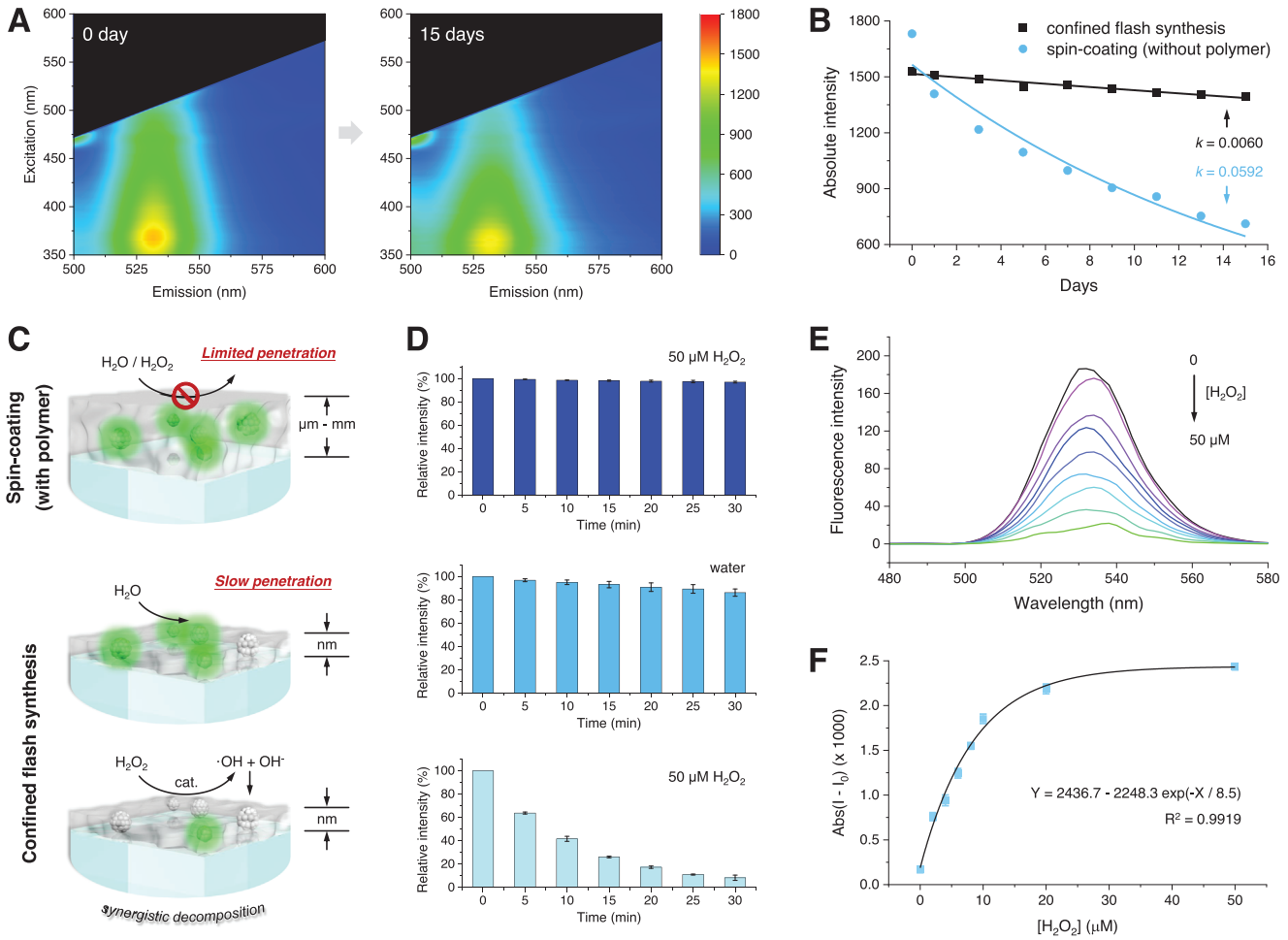

Figure 4. Stability and H_2O_2 response of PQD nanofilm. A) 2D fluorescence spectra of a PQD nanofilm prepared by conFlash synthesis before (left) and after (right) 15 days of storage. B) Fluorescence intensity of PQD nanofilm prepared by conFlash synthesis method and spin-coated PQD film without polymer coating during 15 days storage. The decomposition rate constants were calculated according to the equation of first-order reaction. C) Schematic representation of the H_2O_2 response mechanism of the PQD nanofilm prepared by our conFlash method, in comparison to spin-coated PQD film with polymer coating. D) Relative fluorescence intensity of the PQD nanofilm during 30 min in water (center) and 50 μM H_2O_2 solution (bottom). For comparison, a PQD film with polymer, prepared by conventional pre-synthesis and spin-coating, in 50 μM H_2O_2 solution (top). E) Fluorescence spectra of a PQD nanofilm reacted with different H_2O_2 concentrations. F) Logarithmic relationship between the H_2O_2 concentration in the range from 0 to 50 μM and absolute intensity (Abs(I–I_0)) of a PQD nanofilm. Data are presented as mean ± SD ($n = 3$).

Sekisui Chemical Co. Ltd. Uric acid, NADPH, and phenethylamine were purchased from Sigma Aldrich. Other chemicals were purchased from Alfa Aesar Chemical Co. Ltd. All chemical reagents were of analytical grade and were used directly without further purification. Deionized (DI) water was used throughout.

Donor Slide Fabrication: Glass donor slides with a hematite nano-absorber layer were fabricated using standard microscope glass slides (Marienfeld, Germany) according to our standard protocol.[41] The slides were spin-coated with halide precursor solution using 500 μL solution at 80 rounds per second. For the preparation of halide precursor solution, exemplified for the MABr, 50 mg MABr and 300 mg S-LEC were fully dissolved in a 5 mL mixture of methanol and dichloromethane (v/v = 3:7), forming a homogeneous and clear solution. The MACl, MAI, FABr, CsBr, and mixed halide precursor solutions were prepared with the same formulation at a same molar concentration. The methanol/dichloromethane ratio was optimized before use. The donor slides spin-coated with a $Pb(NO_3)_2$ solution were fabricated with the same parameters: 120 mg $Pb(NO_3)_2$ and 120 mg polyethylene glycol (PEG, MW = 5000) were fully dissolved in 1 mL DI water and spin-coated on glass. The $MnCl_2$, $FeCl_3$, $CoCl_2$, $NiCl_2$, $Zn(NO_3)_2$, and $Y(NO_3)_3$ solutions were used with a same formulation at a same molar concentration. All solutions were used immediately after formulation.

Acceptor Substrate: Three different types of substrates were tested, including standard microscope glass slides, transparent PET sheets (Sigma Aldrich), and ITO-coated glass (Sigma Aldrich). All substrates were used without additional processing except for cutting. The alginate-coated substrates were obtained by spin-coating the substrate with 1 wt% sodium alginate solution using 500 μL solution at 80 rounds per second. The alginate-coated substrates were dried overnight (>10 h) before use.

ConFlash Synthesis of PQDs: The LIFT laser setup was constructed and optimized according to our standard protocol.[42] In a typical experiment, the donor slide, spin-coated with $Pb(NO_3)_2$ solution, and the dry alginate-coated substrate were cleaned by compressed air and fixed on the platform for laser transfer (0.63 mW μm^{-2}, 50 mm s^{-1}). Then, the substrate slide was heated in a self-established glass oven to 100 °C for 60 min under a humid environment of 6 mg cm^{-3}, and washed with 5 mL methanol three times to obtain a substrate with alginate hydrogel patterns. Afterward, the as-obtain substrate with alginate hydrogel patterns and donor slide

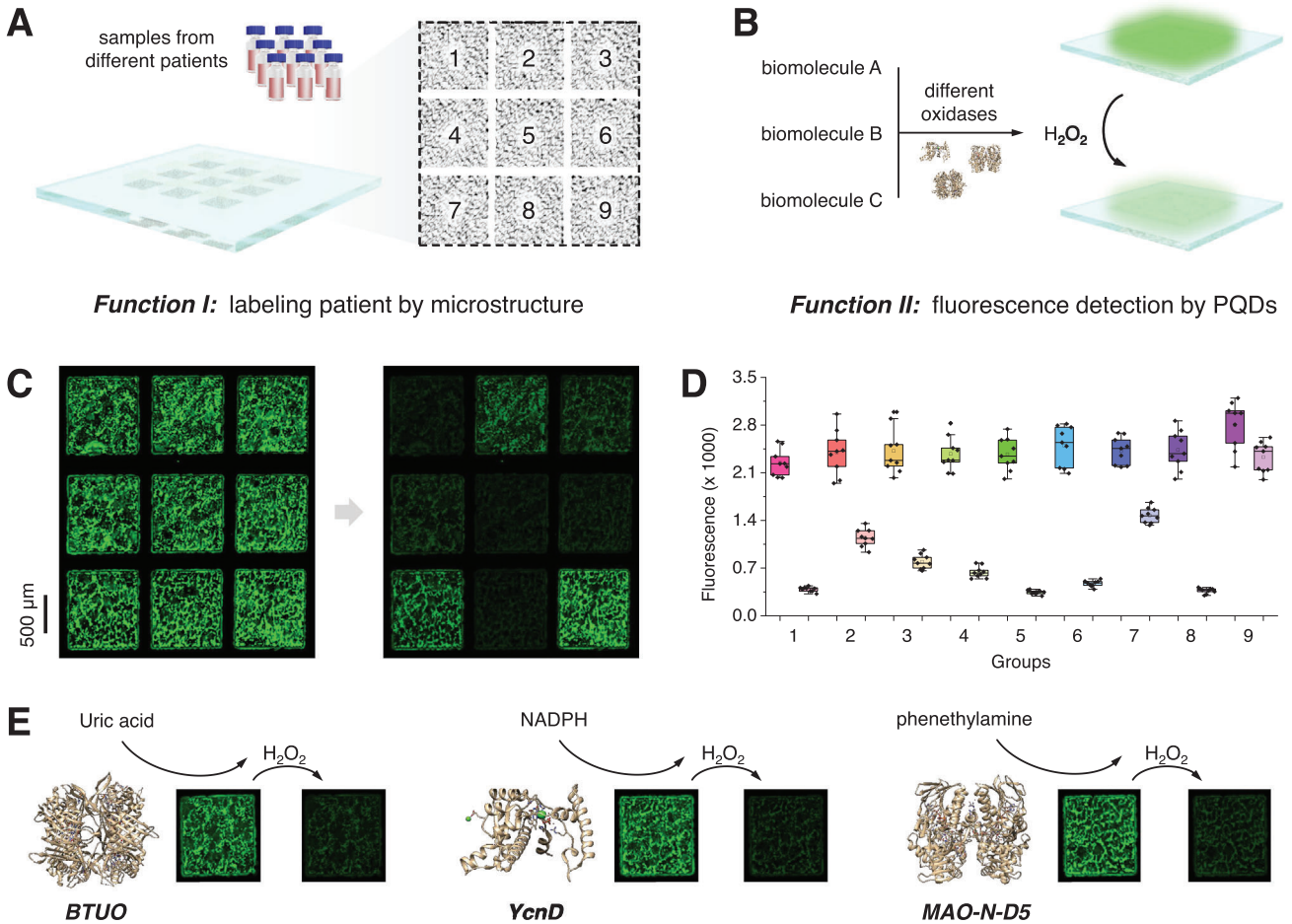

Figure 5. Detection of H_2O_2 and enzyme-based biomolecules by PQD nanofilm. Schematic representation of two functions of PQD nanofilm as A) unique microstructure sample label by and B) biosensor by H_2O_2-responsive fluorescence. C) Fluorescence image and D) fluorescence intensity pre and post reaction of a 3 × 3 PQD nanofilm array responding to different concentrations of H_2O_2. The experiment was double-blind ($n = 9$). Center line, median; square, mean; box limits, upper and lower quartiles; whiskers, 1.5× interquartile range. E) Detection of uric acid, NADPH, and phenethylamine via H_2O_2 quenching of PQD nanofilms functionalized with an engineered urate oxidase (BTUO), a nicotinamide adenine dinucleotide phosphate oxidase (YcnD), or a monoamine oxidase (MAO-N-D5).

spin-coated with halide precursor solution were cleaned by compressed air and fixed on the platform for laser transfer (0.50 mW µm^{-2}, 50 mm s^{-1}).

Solvothermal Pre-Synthesis and Spin-Coating of PQDs as Control: Control PQDs were prepared by a typical solvothermal approach. 3.5 mg of these as-obtained PQDs were dispersed in 5 mL dichloromethane. Standard microscope glass slides were spin-coated with this PQDs dispersion using 500 µL of solution at 80 rounds per second to obtain PQD films without polymer coating. To obtain control PQD films with polymer coating, the as-obtained PQD films were additionally spin-coated with a dichloromethane solution of a styrene-butyl acrylic copolymer (S-LEC, 60 mg mL^{-1}), using 500 µL of solution at 80 rounds per second.

Characterization: The scanning electron microscopy study was carried out using a Zeiss LEO 1550 microscope equipped with a field emission gun and with an Oxford Instruments X-MAX SDD. Energy-dispersive X-ray spectra and surface mapping of the samples were performed during SEM measurements. The morphology of the PQDs formed in the polymer nanofilm was determined using a FEI Tecnai G^{2}F30 transmission electron microscope. The PQDs were removed from the substrate with anhydrous dichloromethane in a N_2-filled glove box and drop casted on the surface of a copper grid. X-ray photoelectron spectroscopy spectra were performed on Thermo escalab 250Xi. UV—vis–NIR transmittance and diffuse reflection spectra were determined on a Hitachi U-4100 UV–vis spectrophotometer. A vertical scanning interferometer (smartWLI compact, Gesellschaft für Bild- und Signalverarbeitung mgH, Illmenau, Germany) was used with 5× and 50× objectives for topographic measurements. Data analysis was carried out in MountainsMap Version 8.0 (Digital Surf, France). The fluorescence images and fluorescence spectra were obtained by Leica TCS SP8X confocal microscopy. The 2D fluorescence spectra and fluorescence lifetimes were taken on a FLS980 lifetime and steady state spectrometer (Edinburgh Instruments). The absolute quantum yield was detected with an integrated sphere executed at the 390 nm. The bare glass slide and pure $MAPbBr_3$ QDs film prepared by pre-synthesis and standard spin-coating method were tested as reference (Figure S23, Supporting Information).

Recombinant Enzyme Expression and Purification: Enzymes sequences and structures are available in the protein data bank (PDB) repository under the accession codes: 5AYJ for BTUO, 1ZCH for YcnD, and 2VVM for MAO-N-D5.

Expression and Purification of Engineered Urate Oxidase from Bacillus sp.TB-90 (BTUO): The synthetic gene encoding for the urate oxidase variant R298C from *Bacillus sp*. TB-90 (BTUO) was subcloned into a pET21a(+) plasmid between NdeI and XhoI restriction sites.[43] The sequence contained a flexible linker (LQNAPAHG) before the XhoI site. *E. coli* BL21(DE3) cells were used as the host organism.

The BTUO expression and purification were performed according to the following procedure. For recombinant expression, 800 mL of lysogeny broth (LB) medium supplemented with ampicillin (100 µg mL^{-1}) were inoculated with 15 mL of an overnight culture of *E. coli* BL21(DE3) cells harboring the desired plasmid DNA. Cells were grown at 37 °C until an OD_{600} of 0.8–0.9 was reached, and the protein expression was induced by the addition of IPTG (0.5 mM). Protein expression was carried out overnight at 25 °C. After harvesting of the cells (4 °C, 10 min, 8944 × g), the remaining cell pellet was resuspended in lysis buffer (50 mM KH_2PO_4, 300 mM NaCl, 10 mM imidazole, pH 8.0) prior to cell disruption by ultrasonication. The protein purification was performed by Ni-NTA affinity chromatography using pre-packed Ni-NTA HisTrap HP columns (GE Healthcare), previously equilibrated with lysis buffer. After loading of the filtered lysate, the column was washed with sufficient amounts of washing buffer (50 mM KH_2PO_4, 300 mM NaCl, 25 mM imidazole, pH 8.0), and bound protein was recovered with elution buffer (50 mM KH_2PO_4, 300 mM NaCl, 200 mM imidazole, pH 8.0). After SDS-PAGE, fractions containing the desired proteins in a sufficient purity (>90%) were pooled and dialyzed against 50 mM K_2HPO_4/KH_2PO_4 buffer (pH 8.0) overnight and concentrated using Centripreps (Millipore). The purified enzyme solution was stored at −80 °C as aliquots after shock-freezing in liquid nitrogen. The final concentration of the protein was determined at 280 nm ($\epsilon_{280} = 36\,390\ M^{-1}\ cm^{-1}$). A typical protein yield of 75 mg L^{-1} cell culture was obtained.

Expression and purification of nicotinamide adenine dinucleotide phosphate (NADP) oxidase from Bacillus subtilis (YcnD): Nicotinamide adenine dinucleotide phosphate oxidase, YcnD, was expressed and purified as previously reported by us.[44]

Expression and Purification of Engineered Monoamine Oxidase from Aspergillus niger (MAO-N-D5): *E. coli* BL21(DE3) cells harbouring a pET28a plasmid encoding for the MAO-N-D5 enzyme were used to prepare an overnight culture (5 mL LB medium supplemented with ampicillin 100 µg mL^{-1}).[45] Next day, 100 µL of the overnight culture were used to inoculate 10 mL of LB medium supplemented with ampicillin 100 µg mL^{-1}. This secondary culture was grown at 30 °C until the OD_{600} reached 0.7–1. Next, 8 mL of this culture were used to inoculate the main culture (800 mL of LB medium supplemented with ampicillin 100 µg mL^{-1}) that was grown at 30 °C overnight without the addition of IPTG (i.e., optimized procedure after expression trials using different conditions).

The solubility tests were performed as follows. The samples were centrifuged at 4500 rpm at 4 °C for 15 min. The supernatants were discarded, each pellet was resuspended in 3 mL Lysis buffer and sonicated (5 min of total sonication time, 10 s pulse on, and 10 s pulse off). In total 1 mL of each lysate was centrifuged for 20 min at 4 °C (14 534 × g). The supernatants and the pellets were analysed with SDS-PAGE. Sample 1 (1000 µL) was taken before overnight expression from the secondary culture when OD_{600} was 0.92. Sample 2 (1000 µL, after 1:5 dilution) was taken after overnight expression from the main culture in absence of IPTG. Samples 3 and 4 were taken from the soluble and insoluble fractions, respectively, after disruption of the cells. Based on the reported molecular weight of MAO-N-D5 (MW: 55.617 Da), it was observed that although the expression of the enzymes seems to be low, the enzyme was found to be in the soluble fraction. Moreover, no enzyme is present in the insoluble fraction. Attempts of purification of MAO-N-D5 with Ni^{2+}-affinity chromatography revealed that the enzyme only eluted in the flowthrough. Due to this fact and the low expression level, the crude lysate was used in this work.

H_2O_2-Response Study: A 50 µM H_2O_2 solution was prepared by diluting 30% H_2O_2 solution in DI water and was used immediately after formulation. 10 µL of 50 µM H_2O_2 solution was deposited on the PQD nanofilm and observed under the microscope. Every 5 min, the fluorescence intensity of the nanofilm was determined. The PQD nanofilm covered with DI water and the spin-coated PQD film covered with 50 µM H_2O_2 solution was used for comparison.

H_2O_2 Determination: The standard solutions of H_2O_2 were prepared by diluting 30% H_2O_2 solution with DI water. All standard solutions were used immediately after formulation. For a typical determination, 10 µL H_2O_2 standard solutions (2.5–50 µM) were deposited on the PQD nanofilms and observed under the microscope. After incubation for 30 min, the fluorescence spectra of all nanofilms were determined, respectively.

Uric Acid, NADPH, and Phenethylamine Determination: The standard solutions (50 µM) of uric acid, NADPH, and phenethylamine were prepared by dissolving analytes in DI water. All standard solutions were used immediately after formulation. As for uric acid determination, 10 µL uric acid standard solution was deposited on the PQD nanofilm modified with BTUO and observed under the microscope. After incubation for 30 min, the fluorescence image of the nanofilm was obtained after removing the uric acid standard solution and drying with compressed air. The fluorescence image for NADPH and phenethylamine determination were obtained by a similar procedure using the PQD nanofilms modified with YcnD and MAO-N-D5, respectively.

Supporting Information

Supporting Information is available from the Wiley Online Library or from the author.

Acknowledgements

The authors thank the financial support from the German Federal Ministry of Education and Research (BMBF, 13XP5050A, F.F.L.), the Max-Planck-Fraunhofer collaboration project (Glyco3Display, F.F.L.), the Max Planck Society, NWO Sector Plan for Physics and Chemistry (F.G.M.), the National Natural Science Foundation of China (82001945, X.Z.), the Shanghai Pujiang Program (20PJ1410700, X.Z.), EU H2020-MSCA-RISE-2017 Action program (CANCER, 777682, H.Z.), and the China Scholarship Council scholarship (202008110184, Z.W.). Y.L. personally thanks Prof. Fuyou Li from Shanghai Jiaotong University and Prof. Zhanfang Ma from Capital Normal University for crucial support and guidance.

Open access funding enabled and organized by Projekt DEAL.

Conflict of Interest

The authors declare no conflict of interest.

Author Contributions

Y.L., F.F.L., F.G.M., and H.Z. conceived the project. Y.L. analyzed the data and wrote the original manuscript. F.F.L., F.G.M., and H.Z. mainly supervised the project, while F.F.L., F.G.M., H.Z., P.H.S, X.Z., and Z.W. acquired the financial support. Y.L., J.Z., and X.Z. designed the methodology for the conFlash synthesis. S.R. and F.F.L. contributed to the establishment and optimization of the laser system. Y.L. performed the synthesis experiments. For enzyme-based biosensing applications, T.K., M.D., and F.G.M. decided, expressed, and purified the enzymes, while Y.L. and Z.W. performed the biosensing experiments. Y.L., F.F.L., F.G.M., and H.Z. decided on the visualization and data presentation. All authors contributed to reviewing and editing of manuscript.

Data Availability Statement

The data that support the findings of this study are available in the supplementary material of this article.

Keywords

biosensor, high-throughput, laser-induced forward transfer, material synthesis, perovskites

Received: July 4, 2024
Revised: August 16, 2024
Published online: September 23, 2024

[1] J. Park, J. Kim, H.-S. Yun, M. J. Paik, E. Noh, H. J. Mun, M. G. Kim, T. J. Shin, S. I. Seok, *Nature* **2023**, *616*, 724.
[2] C. Qin, A. S. D. Sandanayaka, C. Zhao, T. Matsushima, D. Zhang, T. Fujihara, C. Adachi, *Nature* **2020**, *585*, 53.
[3] Y. Zhou, C. Fei, Md. A. Uddin, L. Zhao, Z. Ni, J. Huang, *Nature* **2023**, *616*, 712.
[4] Y. Sun, L. Ge, L. Dai, C. Cho, J. Ferrer Orri, K. Ji, S. J. Zelewski, Y. Liu, A. J. Mirabelli, Y. Zhang, J.-Y. Huang, Y. Wang, Ke Gong, M. C. Lai, L. Zhang, D. Yang, J. Lin, E. M. Tennyson, C. Ducati, S. D. Stranks, L.-S. Cui, N. C. Greenham, *Nature* **2023**, *615*, 830.
[5] C. C. Boyd, R. Cheacharoen, T. Leijtens, M. D. McGehee, *Chem. Rev.* **2019**, *119*, 3418.
[6] H.-S. Yun, H. W. Kwon, M. J. Paik, S. Hong, J. Kim, E. Noh, J. Park, Y. Lee, S. Il Seok, *Nat. Energy* **2022**, *7*, 828.
[7] Q. Jiang, J. Tong, Y. Xian, R. A. Kerner, S. P. Dunfield, C. Xiao, R. A. Scheidt, D. Kuciauskas, X. Wang, M. P. Hautzinger, R. Tirawat, M. C. Beard, D. P. Fenning, J. J. Berry, B. W. Larson, Y. Yan, K. Zhu, *Nature* **2022**, *611*, 278.
[8] Q. Jiang, J. Tong, R. A. Scheidt, X. Wang, A. E. Louks, Y. Xian, R. Tirawat, A. F. Palmstrom, M. P. Hautzinger, S. P. Harvey, S. Johnston, L. T. Schelhas, B. W. Larson, E. L. Warren, M. C. Beard, J. J. Berry, Y. Yan, K. Zhu, *Science* **2022**, *378*, 1295.
[9] Y. Zhao, F. Ma, Z. Qu, S. Yu, T. Shen, H.-X. Deng, X. Chu, X. Peng, Y. Yuan, X. Zhang, J. You, *Science* **2022**, *377*, 531.
[10] K. Xiao, Y.-H. Lin, M. Zhang, R. D. J. Oliver, X. Wang, Z. Liu, X. Luo, J. Li, D. Lai, H. Luo, R. Lin, J. Xu, Yi Hou, H. J. Snaith, H. Tan, *Science* **2022**, *376*, 762.
[11] D. Ma, K. Lin, Y. Dong, H. Choubisa, A. H. Proppe, D. Wu, Y.-K Wang, B. Chen, P. Li, J. Z. Fan, F. Yuan, A. Johnston, Y. Liu, Y. Kang, Z.-H. Lu, Z. Wei, E. H. Sargent, *Nature* **2021**, *599*, 594.
[12] W. Hui, L. Chao, H. Lu, F. Xia, Q. Wei, Z. Su, T. Niu, L. Tao, B. Du, D. Li, Y. Wang, H. Dong, S. Zuo, B. Li, W. Shi, X. Ran, P. Li, H. Zhang, Z. Wu, C. Ran, L. Song, G. Xing, X. Gao, J. Zhang, Y. Xia, Y. Chen, W. Huang, *Science* **2021**, *371*, 1359.
[13] X. Huang, Q. Guo, D. Yang, X. Xiao, X. Liu, Z. Xia, F. Fan, J. Qiu, G. Dong, *Nat. Photon.* **2020**, *14*, 82.
[14] K. Sun, D. Tan, X. Fang, X. Xia, D. Lin, J. Song, Y. Lin, Z. Liu, M. Gu, Y. Yue, J. Qiu, *Science* **2022**, *375*, 307.
[15] C. Chen, J. Chen, H. Han, L. Chao, J. Hu, T. Niu, H. Dong, S. Yang, Y. Xia, Y. Chen, W. Huang, *Nature* **2022**, *612*, 266.
[16] H. Chen, F. Ye, W. Tang, J. He, M. Yin, Y. Wang, F. Xie, E. Bi, X. Yang, M. Grätzel, L. Han, *Nature* **2017**, *550*, 92.
[17] M. Liu, M. B. Johnston, H. J. Snaith, *Nature* **2013**, *501*, 395.
[18] J. Burschka, N. Pellet, S.-J. Moon, R. Humphry-Baker, P. Gao, M. K. Nazeeruddin, M. Grätzel, *Nature* **2013**, *499*, 316.
[19] Y. C. Kim, K. H. Kim, D.-Y. Son, D.-N. Jeong, J.-Y Seo, Y. S. Choi, I. T Han, S. Y. Lee, N.-G. Park, *Nature* **2017**, *550*, 87.
[20] Y. Deng, X. Zheng, Y. Bai, Qi Wang, J. Zhao, J. Huang, *Nat. Energy* **2018**, *3*, 560.
[21] Y. Jiang, C. Sun, J. Xu, S. Li, M. Cui, X. Fu, Y. Liu, Y. Liu, H. Wan, K. Wei, T. Zhou, W. Zhang, Y. Yang, J. Yang, C. Qin, S. Gao, J. Pan, Y. Liu, S. Hoogland, E. H. Sargent, J. Chen, M. Yuan, *Nature* **2022**, *612*, 679.
[22] M. Lai, D. Shin, L. Jibril, C. A. Mirkin, *J. Am. Chem. Soc.* **2022**, *144*, 13823.
[23] Y. Liu, Z. Wei, J. Zhou, Z. Ma, *Nat. Commun.* **2019**, *10*, 5361.
[24] C. Hu, W. Lu, A. Mata, K. Nishinari, Y. Fang, *Int. J. Biol. Macromol.* **2021**, *177*, 578.
[25] Z. Tang, Y. Fu, Z. Ma, *Biosens. Bioelectron.* **2017**, *91*, 299.
[26] Y. Chen, D. Zhang, Z. Wang, M. Tang, H. Zhang, *Adv. Funct. Mater.* **2024**, 2409017, https://onlinelibrary.wiley.com/doi/10.1002/adfm.202409017.
[27] S. Eickelmann, S. Ronneberger, J. Zhang, G. Paris, F. F. Loeffler, *Adv. Mater. Interfaces* **2021**, *8*, 2001626.
[28] Z. Zheng, X. Wang, Y. Shen, Z. Luo, L. Li, L. Gan, Y. Ma, H. Li, A. Pan, T. Zhai, *Adv. Opt. Mater.* **2018**, *6*, 1800879.
[29] R. Ding, C.-K. Liu, Z. Wu, F. Guo, S.-Y. Pang, L. W. Wong, W. Fu Io, S. Yuan, M.-C. Wong, M. B. Jedrzejczyk, J. Zhao, F. Yan, J. Hao, *Nano Lett.* **2020**, *20*, 2747.
[30] J. Zhang, Y. Liu, C. Njel, S. Ronneberger, N. V. Tarakina, F. F. Loeffler, *Nat. Nanotechnol.* **2023**, *18*, 1027.
[31] H. Cho, S.-H. Jeong, M.-H. Park, Y.-H. Kim, C. Wolf, C.-L. Lee, J. H. Heo, A. Sadhanala, N. Myoung, S. Yoo, S. H. Im, R. H. Friend, T.-W. Lee, *Science* **2015**, *350*, 1222.
[32] C. Zhang, B. Wang, W. Li, S. Huang, L. Kong, Z. Li, L. Li, *Nat. Commun.* **2017**, *8*, 1138.
[33] B. Luo, Y. C. Pu, S. A. Lindley, Y. Yang, L. Lu, Y. Li, X. Li, J. Z. Zhang, *Angew. Chem. Int. Ed.* **2016**, *55*, 8864.
[34] A. J. Prochazkova, M. C. Scharber, C. Yumusak, J. Jancik, J. Masilko, O. Bruggemann, M. Weiter, N. S. Sariciftci, J. Krajcovic, Y. Salinas, A. Kovalenko, *Sci. Rep.* **2020**, *10*, 15720.
[35] L. Zhang, P. H. L. Sit, *J. Phys. Chem. C* **2015**, *119*, 22370.
[36] C. Wang, B. R. Ecker, H. Wei, J. Huang, Y. Gao, *J. Phys. Chem. C* **2018**, *122*, 3513.
[37] G. Paris, J. Heidepriem, A. Tsouka, Y. Liu, D. S. Mattes, S. Pinzón Martín, P. Dallabernardina, M. Mende, C. Lindner, R. Wawrzinek, C. Rademacher, P. H. Seeberger, F. Breitling, F. R. Bischoff, T. Wolf, F. F. Loeffler, *Adv. Mater.* **2022**, *34*, 2200359.
[38] G. Paris, A. Klinkusch, J. Heidepriem, A. Tsouka, J. Zhang, M. Mende, D. S. Mattes, D. Mager, H. Riegler, S. Eickelmann, F. F. Loeffler, *Appl. Surface Sci.* **2020**, *508*, 144973.
[39] G. Paris, D. Bierbaum, M. Paris, D. Mager, F. F. Loeffler, *Appl. Sci.* **2022**, *12*.
[40] J. Zhang, Y. Zou, S. Eickelmann, C. Njel, T. Heil, S. Ronneberger, V. Strauss, P. H. Seeberger, A. Savateev, F. F. Loeffler, *Nat. Commun.* **2021**, *12*, 3224.
[41] J. Zhang, Y. Liu, S. Ronneberger, N. V. Tarakina, N. Merbouh, F. F. Loeffler, *Adv. Mater.* **2022**, *34*, 2108493.
[42] S. Ronneberger, J. Zhang, Y. Liu, F. F. Loeffler, *Adv. Funct. Mater.* **2023**, *33*, 2210116.
[43] A. Morokutti, A. Lyskowski, S. Sollner, E. Pointner, T. B. Fitzpatrick, C. Kratky, K. Gruber, P. Macheroux, *Biochemistry* **2005**, *44*, 13724.
[44] T. Knaus, L. Cariati, M. F. Masman, F. G. Mutti, *Org. Biomol. Chem.* **2017**, *15*, 8313.
[45] V. F. Batista, J. L. Galman, D. C. G. A. Pinto, A. M. S. Silva, N. J. Turner, *ACS Cataly.* **2018**, *8*, 11889.